Improved Thermal Signature of Composite Beams with GNP Smart Skin for Defect Investigation

D. Sethy[1] · M. Sai[2] · F. V. Varghese[3] · Krishnan Balasubramaniam[1]

Abstract

In this paper, it is aimed to identify flaws in glass fiber reinforced polymer composites by smart skin graphene nano platelet (GNP) spray coating in infrared thermography technique. The initial resistance of GNP was made to 1 kΩ. Characterization of sensor and beam was done with scanning electron microscopy and computed tomography (CT) respectively. The thermo-elastic behaviour was evaluated in uniaxial test. The surface temperature was studied with IR camera and it was observed that the surface coated GNP sensor upon a damage and without the damage specimen retains heat than without coating the sensor. Hereafter testing with 0.1 mm/min, 0.5 mm/min and 1 mm/min, it was found that without damage specimen, the temperature increased to 112.5%, 13.3% and 40% respectively. And temperature increased to 93.2%, 36.7% and 76.4% in the specimen with the damage. Specimen were also tested for spectrum fatigue cyclic load at 0.1 Hz and 1 Hz. Failure peak of laminates has been analyzed with optical microscopy and CT which was correlated with temperature rise. For 0.1 Hz spectrum loading, the specimen with the damage, with and without GNP coated, temperature rose to 2040% after first laminate failure. Similarly, for 0.1 Hz specimen temperature rose to 15,637.5% in case of without damage specimen, with GNP coated than without GNP coated. And in case of 1 Hz spectrum loading with damage specimen, the temperature rose to 105.73% after GNP coated. Similarly, at 1 Hz loading, the temperature rose to 143.07% in case of without damage specimen after GNP coated. GNP skin coated nano-sensor helps in early detection of temperature signals.

Keywords Polymer-matrix composites · Graphene nanoparticles · Scanning electron microscope · Infrared thermography · Optical microscopy · Computed tomography (CT)

1 Introduction

Glass fiber reinforced polymer (GFRP) has shown good demand in wind energy, aerospace, defence and automotive industry because of its strength, durability and thermal efficiency. However, GFRP based structures in these industries face sometimes high impact damages which are very difficult to inspect in general non-destructive techniques. We normally use NDE technique like IR thermography for damage investigations in the composites. Sometimes signal to noise ratio goes undetectable in case of thermography which can be enhanced clearly by smart graphene nanoplatelet (GNP) material upon spray coating. Therefore, smart carbon allotropy derived sensors are being employed to health monitoring in these structures. Many works on smart composites have been studied with graphene nanomaterials and taking functionalized materials as substrates. Functionalized graphene oxide with octadecylamine was studied for percolation threshold and reinforcement in calculation of ultimate strength. Mechanical properties of graphene were studied and analyzed with brief in bulk composites [1, 2]. Graphene/poly methyl methacrylate (PMMA) based functionalized nanocomposites had been studied for the application of gas sensors, tissue engineering, strain monitoring and drug delivery applications [3]. Piezoresistive behaviour was also studied in polymer matrix composites by spray-coated GNP sensor and maximum gauge factor for GNP was 77 ± 1 [4]. GFRP shows good mechanical properties like good strength to weight ratio, corrosion resistance and

✉ D. Sethy
  debadatta6@gmail.com

[1] Center for Non-Destructive Evaluation, Indian Institute of Technology Madras, Chennai 600036, India

[2] Aircraft Research and Design Centre, Hindustan Aeronautics Limited, Bengaluru 560037, India

[3] Defence Bioengineering and Electromedical Laboratory, Bengaluru 560093, India

fatigue life. However, their inspection concerns a lot for the industry. Sai et al. has developed GNP based strain sensor to detect cracks in simple structures [5]. Here it was mentioned that the magnitude of un-recoverability and change in resistance got reduced with reduction of gauge factor and frequency of cyclic loading. Infrared thermography method is one of them which plays a major role both in an active and passive experiment for flaws detection [6, 7]. It's a non-contact method for acquisition of temperature from surface of any structure in the infrared region and converts it to an electronic signal. Image processing techniques had also been studied for passive and active thermography. Here, thermal signatures are discussed under 1st and 2nd order statistical parameters using neural network classification approach [8]. These are the post-processing techniques after getting the data in a statistical approach, which takes time. Even graphene-based adaptive camouflage had been studied for dynamic control of thermal radiation by altering the optical absorption via the electrical method [9]. Emissivity models had been studied for accuracy in temperature measurement and explained that still, it requires measurement accuracy of radiation thermometer [10]. Evolution of GNPs sensor has broken the record of temperature control as it has got high thermal conductivity of 5000 W/m/K [11, 12]. The surface behaviour of graphene and metal surface interface were studied. Three things matter a lot for bonding between graphene and substrate metal surface which were explained. The binding energy of the d-band center relative to Fermi energy, the distance between graphene and substrate metal surface and lattice mismatching with Moire structure affects thermal emissivity [13]. In Marcus Freitag et al. thermal infrared emission and was found during the emission the least value lies at Dirac point and hence they found wavelength-independent emissivity near-infrared [14]. Even graphene was also fabricated upon the copper substrate to conduct and it showed good result in removing excess thermal heat flux [15]. Even graphene had been enhanced for thermal conductivity by chemical functionalized compounds [16, 17]. Work had been done for energy storage in graphene. Development of sustainable and renewable energy such as solar energy utilizing photovoltaic conversion, photochemical conversion and solar thermal conversion has been studied taking hybrid graphene aerogels into account [18]. Work had been shown taking graphite loading where graphite particles are encapsulated by the polymer matrix and cannot touch each other resulting in low thermal conductivity. They explained thermal conductivity increases with the increase of graphite content [19, 20]. Some experimental and theoretical work was studied for the waviness structure of graphene as per thermal conductivity [21, 22]. Flame resistant material behaviour was studied by using graphene foams as filler that could form the thermal paths in composite even at low filler loadings [23]. Here in this paper, passive thermography technique has been employed. The main parameter used for experimentation is emissivity. So, a slight variation in emissivity brings a large temperature variation. The main engineering art has relied upon the surface paint coating which absorbs the thermal radiation in the infrared wavelength range. Surface paintwork taking graphene as a coating medium provides the best temperature signature [24]. In our previous work, GNPs–GFRP specimens of different resistance were maintained by mechanical exfoliation method and were tested for temperature signature in surface-enhanced glass–epoxy composites [25]. The specimen with 1 kΩ resistance GNP sensor showed the temperature rise of 0.2 °C and on contrary the specimen with 7 kΩ, 21 kΩ and 170 kΩ acted as a sink because temperature densities of GNP in later was less, so, surface temperature couldn't increase.

The goal of study fulfilled in this article is to develop smart polymer nanocomposites with improved thermal signature using spray coated GNPs on GFRP beams and to analyze their thermo-elastic behaviour through IR thermography.

2 Experiment

2.1 Sensor Fabrication and Infrared Thermography Set-Up

GFRP composite of 8-layer specimen (Quasi-Isotropic) symmetric about $(0/+45/90/-45)$ of size 110 mm × 25 mm × 3 mm was prepared via vacuum-assisted resin transfer molding (VARTM) process. While manufacturing GFRP specimen, epoxy-based RIM 135 and RIMH 134 were used as a matrix and hardener, respectively. GNPs (thickness < 2–4 nm; Lateral Size = 5 μm) were obtained generously from GRAPHENE LAB Ltd, London, UK. PMMA (average MW ~ 120 000 g/mol) was purchased from Sigma-Aldrich. Tetrahydrofuran (THF)-AR was used as a solvent.

First of all, 20 mg of GNPs were added into 80 mL of THF and then the solution was ultrasonicated with ELMA Transonic Ti-H-5 bath sonicator, 135 kHz at 80% for 180 min. Then 0.2 mg of PMMA was added to 20 mL of THF and solution was prepared by bath sonicator for 1 h. Then the two solutions (GNP + THF + PMMA) were mixed to make a single solution and was sonicated for 2 h. Then the solution was equally distributed to two GFRP specimen (with damage GNP coated and without GNP coated specimen) by spray coating under the marked area (30 mm × 20 mm) on GFRP specimen by a spray gun using nitrogen gas.

Then the specimens were dried for 1 h at 40 °C. Experimental setup to measure the surface temperature of the GNP–GFRP beams under load is shown in Fig. 1b.The specimen was loaded in the Instron Universal Testing machine,
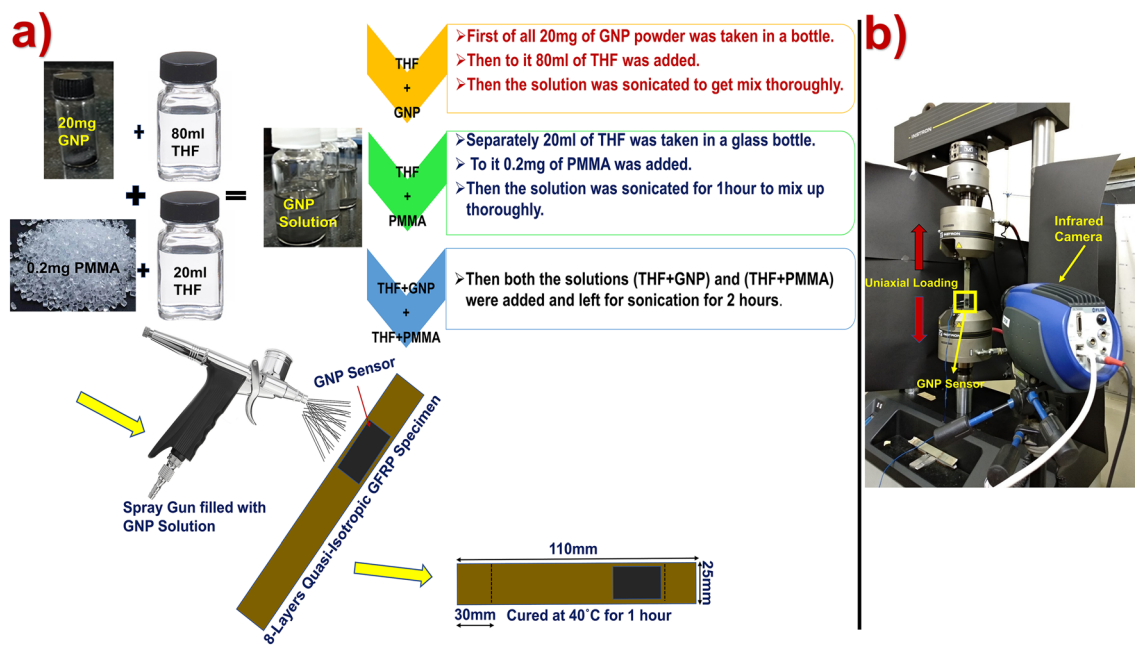
Fig. 1 **a** Fabrication of GNP smart layer on GFRP composite beams (A small area of 30 mm×20 mm size was chosen at the center of GFRP composite (with damage and without damage region)) **b** Experimental setup to measure the surface temperature of the blank specimen (with and without damage) and GNP coated specimen (with and without damage) beams under mechanical loading through Infrared Camera

an IR camera (*SC7000; FLIR* Systems, sensitivity~20 mK) was placed on a tripod to detect the infrared radiation emanating from the GNP layer.

The data from the IR camera was processed in Altair software to obtain the temperature and the thermograms.

3 Characterization

3.1 SEM, Raman Study and CT

GNP coated GFRP specimen was subjected to SEM (*INSPECT F-50*) to assess the morphology of the spray-coated sensors at different resolutions. In Fig. 2a, at 200 μm, the laminates of GFRP with coated GNP sensor can be seen. The channel type of slot, as can be seen, is nothing but the surface adhered with GNP sensor. In Fig. 2b, the lumped platelets as shown are the sensors oriented randomly because of several layers of spraying upon GFRP. While spraying the maximum number of GNPs adhered to trenches and ridges of GFRP composite specimen.

The sensor was prepared with an electrical resistance of 1 kΩ (measured by *Keithley Sourcemeter* (2450)) and sprayed to get adhered upon GFRP specimen. In Fig. 2c and d, the GNP sensor can be seen at the resolution of 1 μm and 500 nm. These sheets are GNPs which act as a sensor for heat conduction. Raman spectroscopy is a smart NDT

technique for the characterization of GNP. Figure 2e shows the Raman spectrum of GNP used in this study, which is characterized by the number of graphene layers and the existence of defects. G peak (~ 1560 cm^{-1}) and D peak (~ 1367 cm^{-1}) can be observed from the above Fig. 2.

G band occurs when GNP is stacked one upon the other, the relative motion between the GNP flakes leads to vibration of the lattice. The D band is due to the breakage of translational symmetry during the solar exfoliation process. Similarly, the 2D band (G'peak) was also seen at~2734 cm^{-1} due to second-order zone boundary phonons. Here taking the degree of graphitization, it was found out to be 0.87, as the ratio of I_D/I_G. The spot from which GNP flakes were characterized is shown above in Fig. 2. GNP coated specimens, as shown in Fig. 3a and b, were tested in CT before uniaxial loading. Here the fibers were of good condition both in without damage specimen and with damage specimen. The fibers around the damage were of good condition as can be seen in Fig. 3a and b. There was no gap in between the fibers.

Then the specimens were tested under uniaxial loading at a displacement rate of 0.1 mm/min, 0.5 mm/min and 1 mm/min. GNP coated specimen with damage and without damage were tested at different displacement rates of 0.1 mm/min, 0.5 mm/min and 1 mm/min. Then after each batch of strain testing for GFRP specimen, it was subjected to CT scan (Phoenix Vtomex industrial high-resolution CT and X-ray system, equipped with 240 kV/320 W
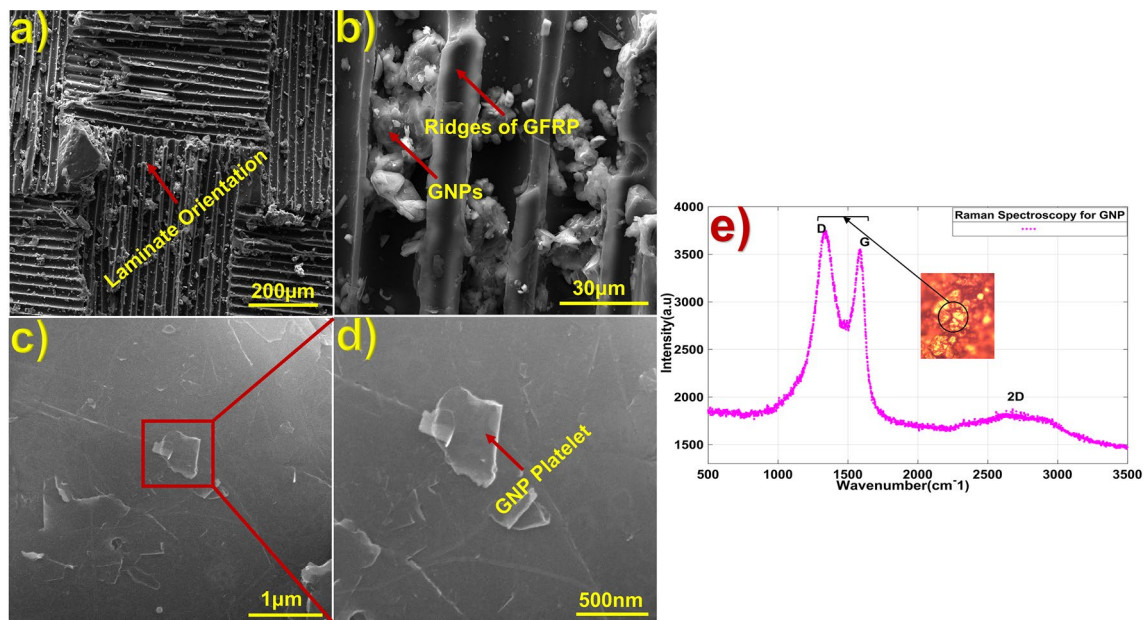
Fig. 2 SEM images of GNP coated specimen at a different resolution: **a** GNPs coated upon GFRP at 200 μm. **b** Stack of GNPs adhered to ridges and valley of GFRP composites **c** and **d** GNP sheet at the nanometer level **e** Raman spectroscopy for the identification of GNP (spot image of laser source taken at the surface GNP)

high-power microfocus X-ray tube) to see the morphology change inside fibers of GFRP. As seen from Fig. 3, GFRP specimen with a damage of 1 mm diameter was tested for strain action at different displacement rates like 0.1 mm/min, 0.5 mm/min and 1 mm/min. At 0.1 mm/min, fibers debonding was very small, as compared to a higher strain rate of 0.5 mm/min and 1 mm/min. At 0.5 mm/min the fibers got dislocated away from each other and at 1 mm/min the fibers developed gaps because of fibers breakage and debonding action with the matrix. This because of straining action which breaks the fiber and during this stage of slow static action, energy is absorbed. With the increment of displacement rate at 0.5 mm/min as seen from in 3d, delamination took place in which fibers got detached from each other and developed gap in between. Again, with an increment of displacement rate at 1 mm/min, the fibers developed a gap in between the fibers fully.

Similarly, in Fig. 3f–h there is also the generation of delamination and debonding with the propagation of displacement rate. This stage is the release of energy in terms of heat. During straining action, the matrix developed cracks and it reaches to fibers slowly which leads to a release of energy in terms of temperature. The fibers develop heat because of friction during strain that leads to damage of resin and hardener and leads to complete damage of fiber bonding. Strain also leads to elongate the fibers and hence leads to breakage of fibers. Blank specimen with and without damage, with GNP coated and without GNP coated were subjected to uniaxial loading up to 5 kN.

As seen from the Fig. 4a, blank specimen was tested for 0.1 Hz spectrum fatigue load. After testing, cracks and delamination developed which resulted in the fibers and matrix to pull out from each other. Side view of Fig. 4a shows the laminate's breakage and buckling phenomenon due to weak in compressive loading.

Similarly, in Fig. 4c, maximum damage occurred as compared to Fig. 4a, because of reduction in the stiffness of the specimen in presence of a damage. Figure 4d is the side view of Fig. 4c which shows fiber breakage and delamination. Completely five layers separated from the parent specimen due to fiber breakage inside laminates. Similarly, in the case of 1 Hz spectrum loading, the propagation of crack is more as compared to the 0.1 Hz specimen testing. From Fig. 4e (with damage), there is complete fiber breakage at 1 Hz but incase of 0.1 Hz the fiber breakage was not from central part but near to the gripper end. From Fig. 4f, there is the visibility of complete delamination of fibers and severe buckling that led to rise in fibers because of friction between the laminates.

As seen in Fig. 4g and h (without damage), there is complete fiber pull out because of rapid crack growth that led to the fiber breakage. All these crack growths inside the fibers led to friction which released temperature and was captured with IR-thermal camera for quantitative analysis.
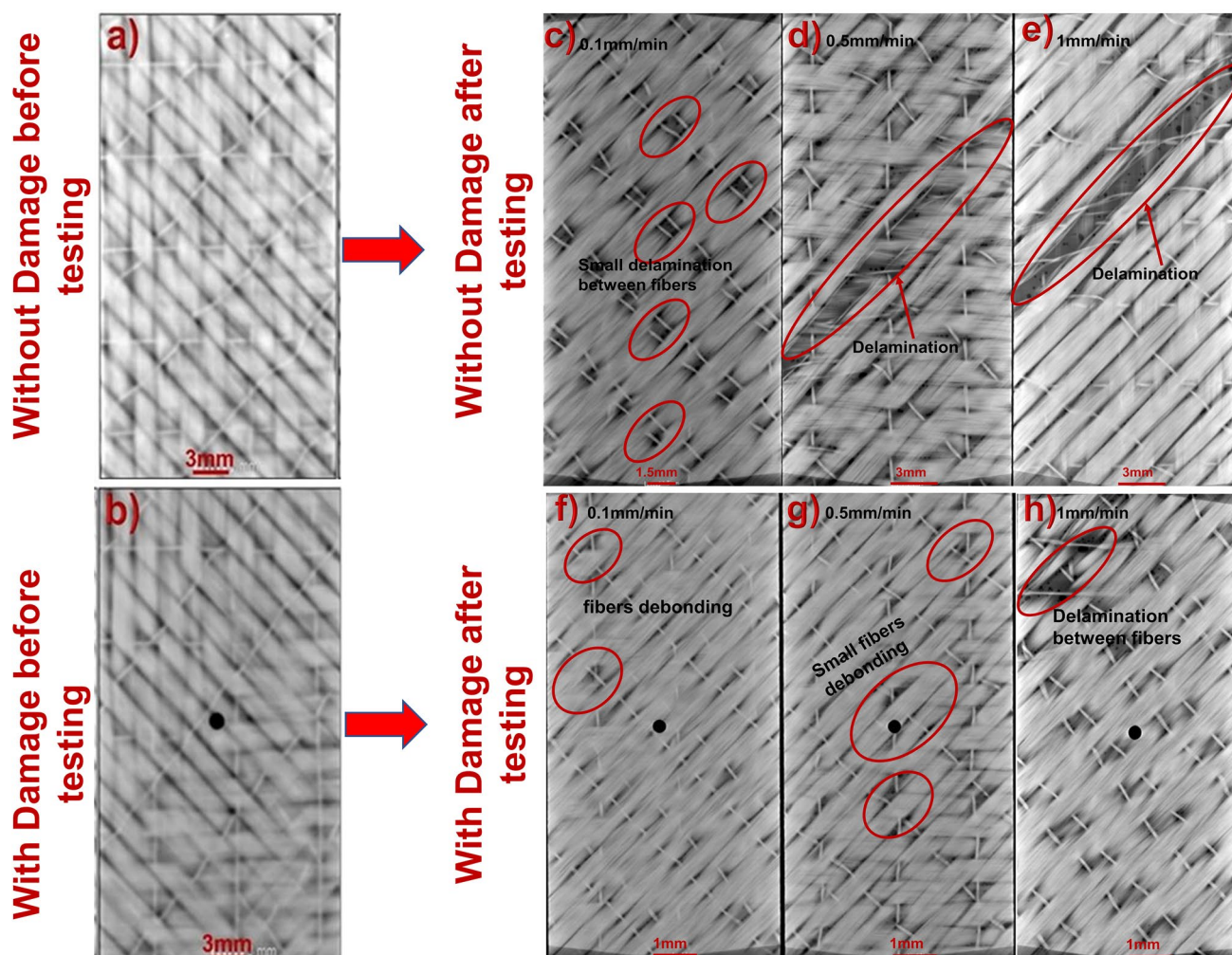
Fig. 3 Computed Tomography (CT) of GNP coated GFRP composites during static loading: **a** and **b** GFRP specimen of 110 mm × 25 mm without a damage and a damage of 1 mm at the center before testing. **c**, **d** and **e** GFRP composite plate without a damage after testing at 0.1 mm/min, 0.5 mm/min and 1 mm/min respectively shows delamination. **f**, **g** and **h** GFRP composite plate with damage after testing shows fibers debonding and delamination at 0.1 mm/min, 0.5 mm/min and 1 mm/min respectively

4 Results and Discussion

4.1 Uniaxial Loading

Similarly, blank specimen with and without the damage when were subjected to strain uniaxial loading, change in temperature decreased down to − 2.47 °C and − 1.6 °C respectively. As GNP has good thermal conductivity, GNP coated specimen conducts heat during the time of monotonic loading. Figure 5c–e show the thermograms with multi-view images of progressing nature of blank specimen with an increment of time. As seen from the Fig. 5c, the blank specimen shows brightness (surface temperature) initially, but at end of the testing i.e. after 200 s, the brightness is reduced indicating a drop in the temperature. But from Fig. 5f–h, heat is absorbed by graphene which is detected by IR camera and the temperature change is reduced. Similarly, blank specimen with damage and GNP coated specimen with damage can be seen from Fig. 5i–n respectively.

The mechanical work subjected to GFRP up to 5 kN get absorbed by the specimen and this heat passively is captured by infrared thermography camera. The GNP coated specimen elongates under uniaxial loading and shearing action takes place among the GNPs which stuck to the beam surface and also in between the GNPs layer. This leads to the heating of the GNPs [26]. The main reason behind friction in graphene apart from the external active source is the electro-phonon coupling and wrinkling of the graphene surface. They are the reasons for thickness dependence of graphene friction which influence the change in substrate morphology. Since GNPs are the good conductors/emitters of heat, a rise in the temperature is observed with the load. As seen in Fig. 3, the fibers are delaminated which leads to the release of energy in terms of temperature. Similarly, in Fig. 6, the

Fig. 4 Computed Tomography (CT) of GNP coated specimen during dynamic spectrum loading: **a** and **c** GFRP specimen of 110 mm×25 mm without a damage and a damage of 1 mm at the center respectively, after testing of 0.1 Hz. **b** and **d** side view of GFRP. **a** and **c** respectively, showing delamination and cracks after 0.1 Hz spectrum loading. **e** and **g** GFRP composite plate with damage and without damage respectively, after testing shows fibers debonding and delamination at 1 Hz. **f** and **h** side view of GFRP **e** and **g** respectively, showing delamination and cracks after 1 Hz spectrum loading
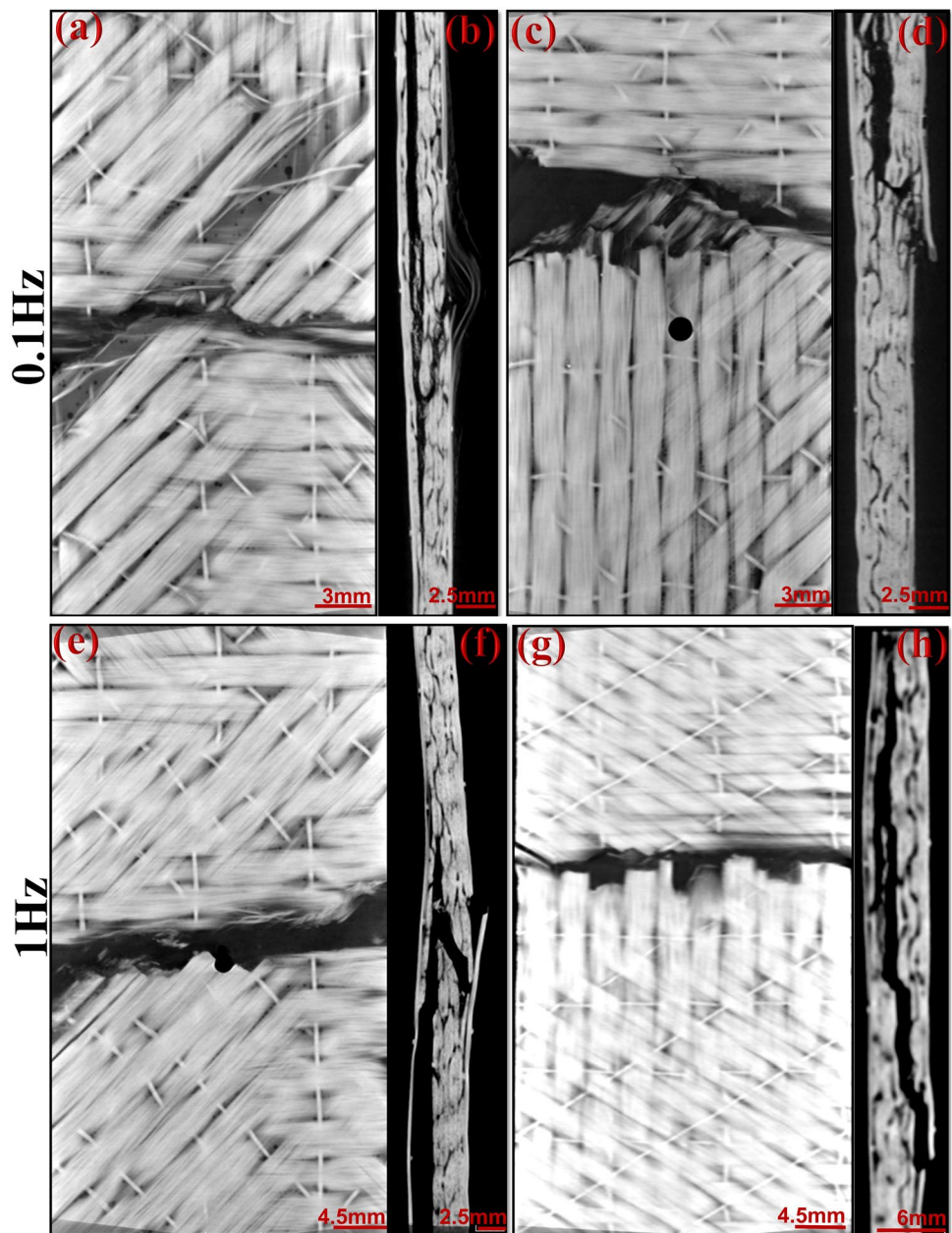
temperature slopes down with increment in displacement rate at 0.5 mm/min. Specimen with GNP without damage sloped down to −0.135 °C. Specimen with GNP with the damage, the temperature signal slowed down to −0.15 °C. Correspondingly samples without GNPs and without damage, the temperature went down to −0.151 °C with an increment of displacement rate. And specimen without GNP with damage, temperature went down to −0.237 °C. With the increment of displacement rate, there is more fiber pull out [27]. As there is more fiber pull out as can be seen from Fig. 3, the energy got released and from inside fibers of the layers to the surface, temperature takes longer time to get conducted. So, as compared to GNPs coated specimen,

the samples without GNPs coating conducts less temperature. With the development of extreme fibers pulls out and delayed growth rate, there is a dissipation of energy which takes longer time to reach the surfaces. As GNPs are good conductor of heat, so the temperature gets absorbed after the release of energy from GFRP inner fibers to surface [28]. So, the temperature is taking more time to get conducted by GNPs as the temperature has to travel from inner fibers to surface. From Fig. 6c–e, blank specimen thermograms has been shown till 35 s, which shows drop in the surface temperature as temperature is lost to the surrounding.

In Fig. 6f–h, thermograms have been shown for GNPs coated specimen and specimen for the displacement rate of
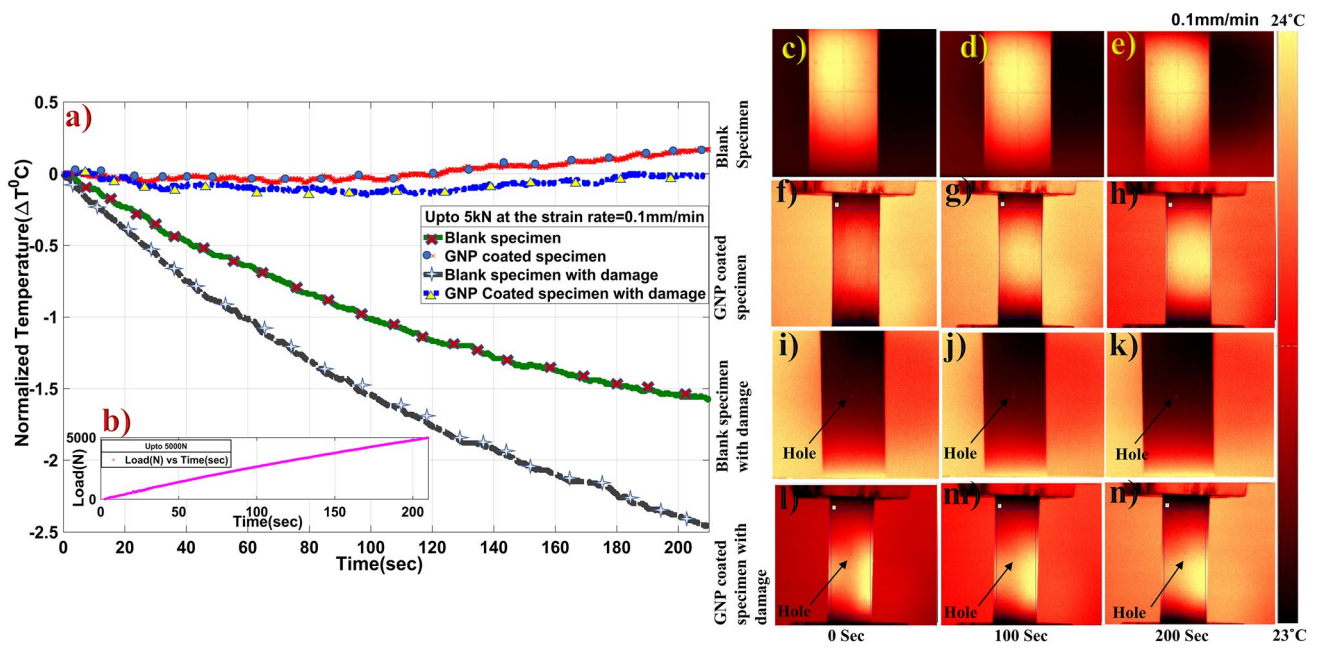
Fig. 5 Normalized Temperature by Infrared Thermography: **a** Blank specimen and GNP coated specimen of 110 mm×25 mm (with a damage of 1 mm) at the center and without damage). **b** Uniaxial Loading upto 5 kN at the strain rate of 0.1 mm/min. Thermograms image at 0 s, 100 s and 200 s for displacement rate at 0.1 mm/min.

c, **d** and **e** Blank specimen. **f**, **g** and **h** GNP coated specimen. **i**, **j** and **k** Blank specimen with a damage. **l**, **m** and **n** GNP coated specimen with damage ((1 mm at the center) (damage may not be visible because of colour contrast)) (Color figure online)
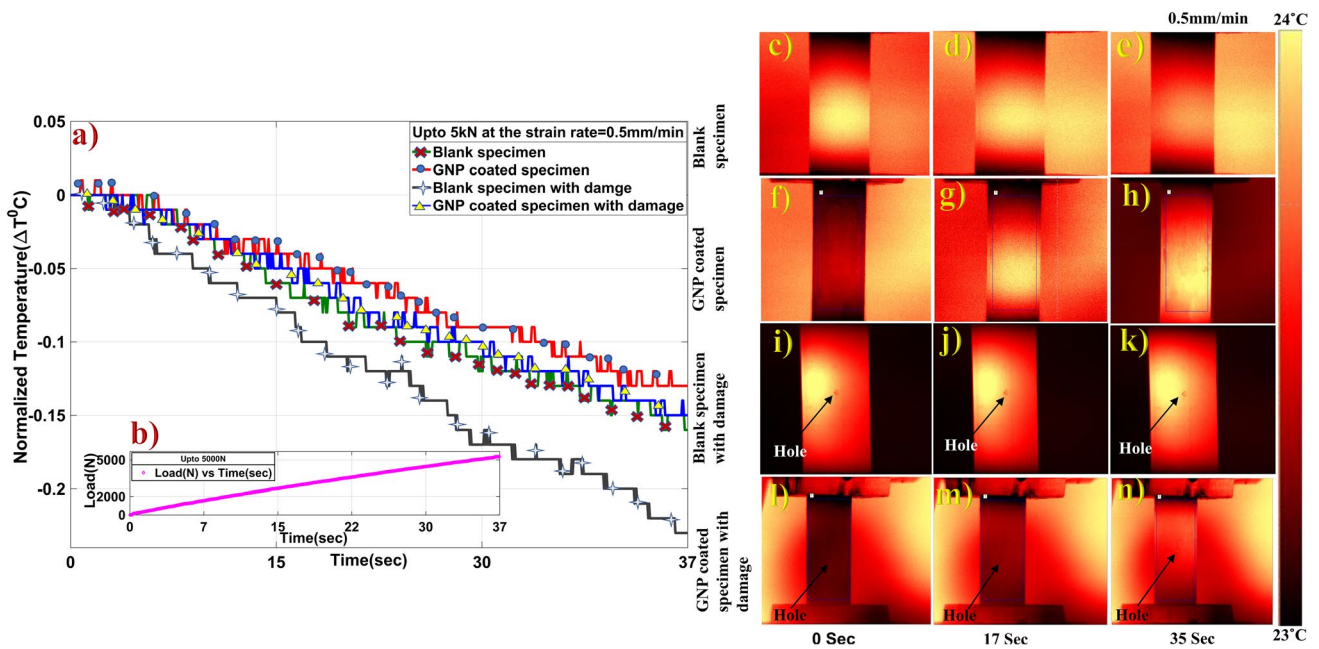

Fig. 6 Normalized Temperature by Infrared Thermography: **a** blank specimen and GNP coated specimen of 110 mm×25 mm (with a damage of 1 mm) at the center and without damage). **b** Uniaxial Loading up to 5 kN at the displacement rate of 0.5 mm/min. Thermograms image at 0 s, 17 s and 35 s for displacement rate at 0.5 mm/

min. **c**, **d** and **e** Blank specimen. **f**, **g** and **h** GNP coated specimen. **i**, **j** and **k** Blank specimen with damage. **l**, **m** and **n** GNP coated specimen with a damage ((1 mm at the center) (damage may not be visible because of colour contrast)) (Color figure online)

0.5 mm/min. In this, there is a rise in temperature in case of GNP coated specimen as compared to blank specimen. This shows at the end of 35 s there is drop in temperature on the specimen surface and temperature is absorbed. So, there is less temperature decrement as compared to blank specimen. In blank specimen temperature goes missing to surrounding which can be captured by coating GNP. Similarly, blank specimen with damage and GNP coated specimen with damage can be seen from Fig. 6i–n respectively.

Similarly, as seen from Fig. 7a and b, testing was done for 1 mm/min and loading took 18 s to complete. The temperature slopes went down for GNP coated specimen without damage to − 0.15 °C and for GNP coated specimen with the damage, the temperature went down to − 0.16 °C. For blank specimen, the temperature sloped down to − 0.25 °C and for blank specimen with the damage, the temperature sloped down to − 0.68 °C. As seen from Fig. 7f–h, at the displacement rate of 1 mm/min, for the GNP coated specimen the colour transition kept on decreasing from 0 to 18 s but as compared to GNP coated specimen with the damage from Fig. 7l– n, the thermograms colour transition is little brighter. Similarly, blank specimen with damage and GNP coated specimen with damage can be seen from Fig. 7c–e and i–k respectively. From Fig. 11, tabulation for quantitative analysis at different uniaxial loading rate has been shown. During the time

of uniaxial loading, the fibers got delaminated and with a progressive increment of straining action the interface between fibers-matrix with GNP gets separated and hence the thermal conductivity is affected. As GNP is adhered to the surface of GFRP, so because of straining action, lattice vibration comes into action which makes GNP to re-orient towards the direction of force applied. During this orientation, thermal energy is transferred in the form of lattice vibration called phonons. Therefore, the lattice vibration develops poor coupling modes in between GNP/GFRP composite fiber and matrix [29, 30]. This leads to the development of thermal resistance called Kapitz resistance [31]. So, GNP coated specimens with and without damage conduct more temperature as compared to neat GFRP specimen. And with an increment of displacement rate, the thermal conductivity got reduced as conductivity gets affected by Graphite orientation. During the testing because of change in the orientation of GNPs the conductivity gets affected as the network of alignment between GNPs change themselves. Also, defects arouse in GNPs because of delamination generated between the GNP-GFRP surface interfaces which leads to the development of lattice vibration called phonons. This leads to phonon scattering. And though phonon scattering affects the flow of electrons. And with defects electron, thermal conductivity also gets reduced [32].
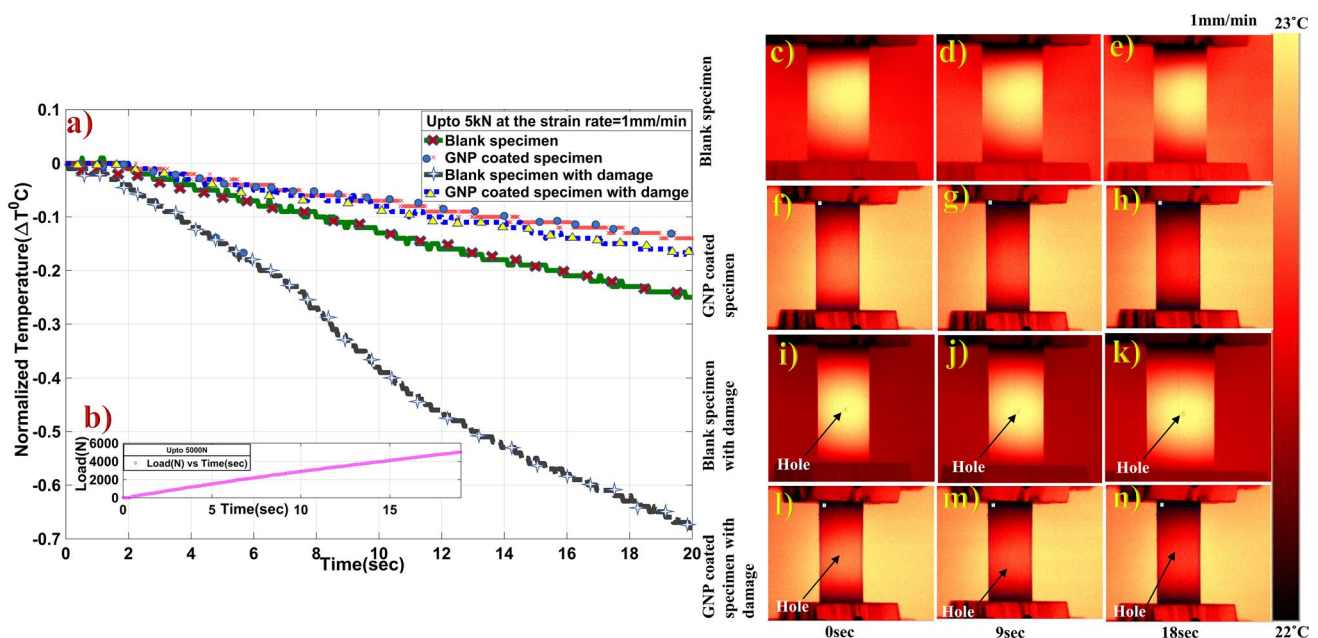

Fig. 7 Normalized Temperature by Infrared Thermography: **a** blank specimen and GNP coated specimen of 110 mm×25 mm (with a damage of 1 mm at the center and without damage) **b** Uniaxial Loading up to 5 kN at the strain rate of 1 mm/min. Thermograms image at 0 s, 9 s and 18 s for the strain rate of 1 mm/min. **c**, **d** and **e** Blank specimen. **f**, **g** and **h** GNP coated specimen. **i**, **j** and **k** Blank specimen with damage. **l**, **m** and **n** GNP coated specimen with damage ((1 mm at the center) (damage may not be visible due to colour transition)) (Color figure online)

4.2 Spectrum Loading (Position Control Mode) at 0.1 Hz and 1 Hz

Glass fiber composites are very much weaker under spectrum loading as the resistance of the fiber matrix is lower in case of glass fiber. In case of cyclic tensile-compressive loading, first of all, fiber breakage initiates and later propagates through the matrix which marks the end of initiation with fibers pull out at the end. Fibers inside the GFRP loose geometrical stability in continuous tensile-compressive loading which leads to the development of bending and buckling of fibers. Failures are interlaminar to translaminar in fatigue loading which are the characteristics for glass fiber strands breakage to individual breakage of fibers. These are only observed in case of fatigue failure which is absent in monotonic loading where only fiber pullout takes place. So, in fatigue, there are more chances of friction between the fibers and matrix than monotonic loading. This friction leads to temperature rise in between the fibers that leads to temperature release to surroundings. As GNP sensor has been fabricated on the GFRP skin, the temperature is absorbed and is dissipated to surrounding nicely. GNPs are good conductor and emitter of heat. As shown from the Fig. 8, blank specimen and GNP coated specimen were tested at 0.1 Hz and 1 Hz with damage and without a damage at Instron Machine 8801 (load-bearing capacity of $\pm$ 100 kN) in wave-matrix software.

Here 22 blocks were designed at different cycle number with different position (mm) amplitude keeping the frequency constant 0.1 Hz and 1 Hz respectively as shown in Fig. 8a. As seen in Fig. 8, optical microscopy was taken to analyze the surface damage at a different magnification of different frequencies being tested. From Fig. 8b, c, f and g, black coating shows the presence of GNPs sensor fabricated upon GFRP specimens which are absent in Fig. 8d, e, h and i. Here damages like delamination, matrix roller and in-plane shear damage can be seen. At 10x magnification from Fig. 8b, with the presence of damage, fibers and matrix get ruptured as can be seen which is a combination of both opening and shearing mode. Here stress gets concentrated at the edge of damage which can be seen at 20x magnification without GNP coating with the damage from Fig. 8d. Similarly, without the GNP coat, from Fig. 7c, only 'matrix rollers' can be seen after testing at 10x. Also, there is delamination from the 1st laminate surface which can be seen at 20x magnification at Fig. 8e. Similarly, when the frequency was increased to 10 times of initial spectrum loading with position control mode to 22 cycles, it was observed that GNP coated with damage specimen at 1 Hz shows maximum rupture as there was more fiber pull out and severe damage in the form of matrix rollers and delamination cause more
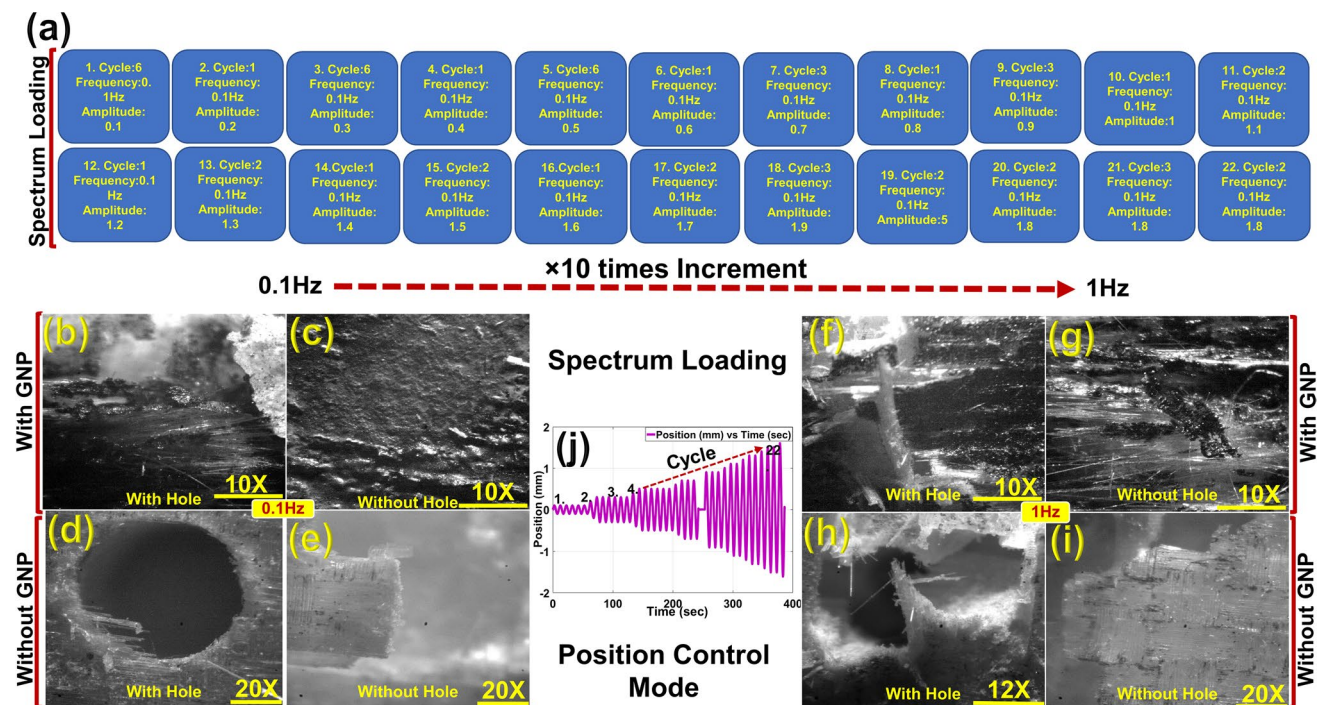

Fig. 8 Spectrum loading block diagrams for testing with frequency of 0.1 Hz and 1 Hz: **a** Block models for to start with cyclic load at different parameters (cycle no., frequency and amplitude).**b**, **c**, **d** and **e** CT image at 0.1 Hz for GFRP and GNP coated specimen with damage and without damage. **f**, **g**, **h** and **i** Optical Microscopy image at 1 Hz for GFRP and GNP coated specimen with damage and without damage

friction that leads to higher temperature rise as shown in Fig. 9. Near to the edge of the damage from Fig. 8h, as compared to Fig. 8d, there is much damage from in-plane shear which leads to delamination and fiber pullout. Similarly, from Fig. 8g and h, with and without GNP coating without the damage, at 10x and 20x respectively, there is much rupture in fibre breakage and surface delamination that leads to complete failure of GNP. A set of 4 batches of the sample were tested. Two sets of GNP coated specimens for 0.1 Hz (with and without damage) and two sets of blank specimens (with and without damage)). Similarly, another batch was tested for 1 Hz. As seen from above Fig. 8, four batches of sample namely GNP coated specimen (with and without damage) and blank specimen (with and without damage) were tested at 0.1 Hz. As seen from the Fig. 8b, c and d, position vs time and load vs time have been shown where the damage can be identified after 200 s from mechanical testing as there was a discontinuity in the cycle.

From Fig. 8c with damage specimen, it is seen that failure takes place after 270 s which is delayed in case of without damage, which took 380 s. It is because of stiffness failure. As a result of which there is more stress concentration at the edge of damage specimen, that leads to release of energy in terms of temperature, which was captured by IR-thermography with the help of skin coated GNP sensors. As seen from the above Fig. 9e and f, for specimen GNP coated specimen and blank specimen, w.r.t to mechanical loading, failure can be observed from the information of position and load. For

the specimen with the damage, failure can be observed from load vs. position data. For the sample GNP coated specimen with damage, 1st peak of failure was observed from the first laminate of the surface at position 0.696 mm and load 8.02 N following 2nd peak of failure at 0.70 mm and 8.57 N. Then complete failure took place at 0.99 mm and 1.49 N. Load decreases here because of complete reduction in stiffness. Also, at a nano-level, the temperature data from GNP coated specimen reveals the time confirmation of the breakage of GFRP fibers in terms of temperature release from GNP coated skin captured by IR-camera from its surface. As shown from the Fig. 9a, GNP coated specimen with damage shows 1st peak level of fiber breakage which was at 210 s with an increment of 9.63 °C. Then 2nd peak released temperature 8.98 °C following the 3rd peak of failure at 10.66 °C. And the complete failure of fibers took place at 9.89 °C which marked the complete reduction in the release of temperature. Similarly, for GNP coated specimen without the damage, temperature released was 12.43 °C. 2nd peak of failure was observed with temperature release of 3.68 °C following the third peak of failure at 10.68 °C and completely failed with temperature releasement of 4.46 °C. For specimen without GNP without the damage, 1st peak of failure was observed at 0.08 °C following 2nd peak of failure at −0.85 °C. Then 3rd peak of failure was observed at 2.2 °C following the extreme rise in temperature at 29.3 °C in 4th peak. Then the temperature was reduced to 19.27 °C when failure took place in the form of delamination and failed
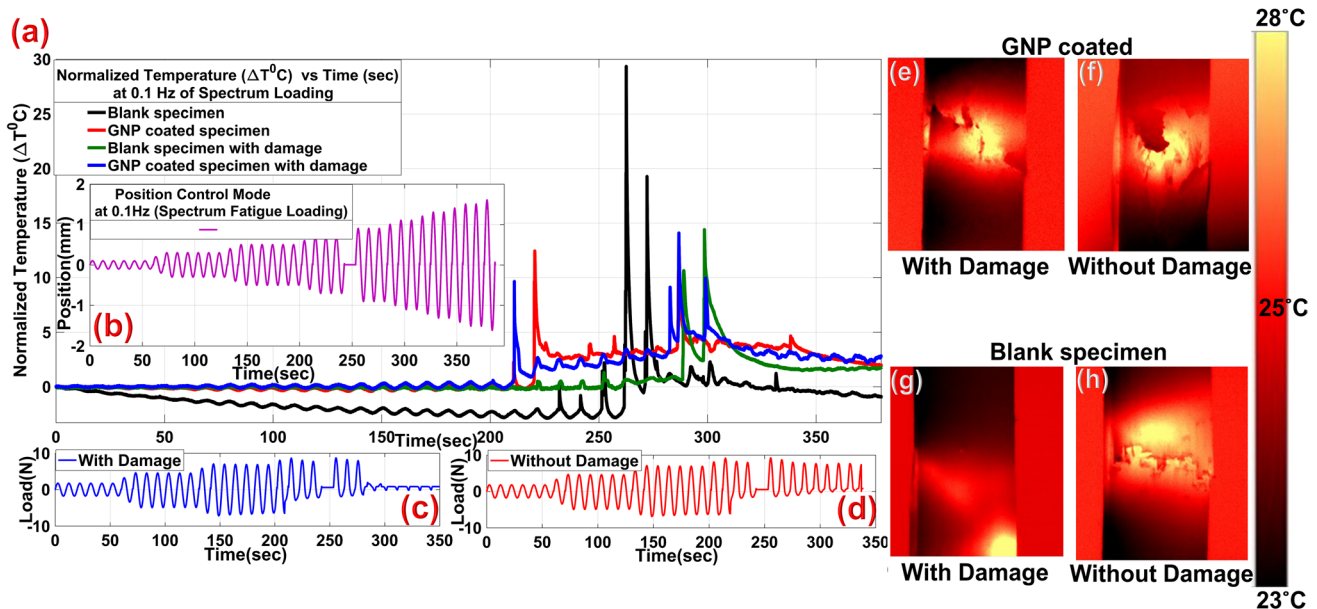

Fig. 9 Normalized temperature monitoring of GFRP at 0.1 Hz of spectrum loading: **a** blank specimen and GNP coated specimen of 110 mm×25 mm (with a damage of 1 mm at the center and without damage) tested for Normalized temp vs Time. **b** Position vs Time during spectrum fatigue at position control mode. **c** and **d** Load vs Time graph till the failure for GNP coated specimen with and without damage for indication of failure. **e** and **f** GNP coated specimen with and without damage till break in spectrum loading. **g** and **h** Blank specimen with and without damage for spectrum loading upto break

with the release of temperature at 1.23 °C. For specimen without GNP with the damage, 1st peak for temperature rise was observed at 0.46 °C following 2nd peak for temperature rise at 0.49 °C.

Similarly, 3rd peak for temperature rise was observed at 0.55 °C but after then because of delamination temperature suddenly rose to 10.63 °C. Following the maximum fiber breakage with the release of temperature 14.39 °C and then complete damage took place with temperature release of 3.35 °C. Correspondingly, a thermogram can be observed for the specimen with GNP and without GNP coated upon GFRP with and without damage specimen in Fig. 9e, f, g and h revealing the surface temperature released during fibers breakage. From the above Fig. 10b, position vs time has been shown, which took 45 s to complete. From Fig. 10c and d, load vs time w.r.t damage has been shown, where failure took place at 39th s and it took 42nd s for specimen without the damage respectively. As seen from the above Fig. 10e and f the failure of the specimen with the damage in mechanical fatigue testing was observed to be at 0.8966 mm and 9.10 N following the 2nd peak of failure at 0.9 mm and 8.215 N. The 3rd peak was observed at 0.9 mm and 7.26 N following the complete failure at 1.05 mm and 3.2 N. Correspondingly, it was observed for temperature peak rise level with an increment of amplitude in spectrum fatigue loading. As seen from above Fig. 10a for the GNP coated specimen with the damage, temperature peak for

1st laminate failure occurred at 17.46 °C following the 2nd peak of failure with the release of temperature at 17.62 °C and maximum temperature is released in 3rd peak at 22.41 °C. Then complete failure took place with the release of temperature 17.38 °C. Similarly, for GNP coated specimen without damage, 1st failure was observed with the release of temperature 12.81 °C following 2nd peak rise in temperature 32.7 °C. The complete failure took place with the release of temperature 19.57 °C. Similarly, blank specimen was tested for mechanical fatigue loading. The 1st peak for laminate failure took place at 0.903 mm and 10.45 N following 2nd peak of failure at 0.902 mm and 9.56 N. The complete fiber breakage took place at 1.09 mm and 7.7 N following the complete failure at 1.2 mm and 4.49 N. Correspondingly comparing in terms of temperature, blank specimen without damage for 0.1 Hz, 1st peak of temperature rise was 5.21 °C and then it decreased down to failure 4.44 °C. Similarly, for the specimen with the damage, 1st peak for failure in the laminate was observed with 4.43 °C following 2nd peak at 28.49 °C and then complete failure was observed with reduction of stiffness with temperature 17.41 °C. At 1 Hz, for specimen without GNP without the damage, 1st peak failure was observed at 5.19 °C following the complete failure at 4.24 °C. But for the sample without GNP with the damage, 1st peak was observed at 4.71 °C following 2nd peak of failure at 5.3 °C. Then 3rd peak of failure was observed at 28.49 °C following the complete failure at 4th peak 15.75
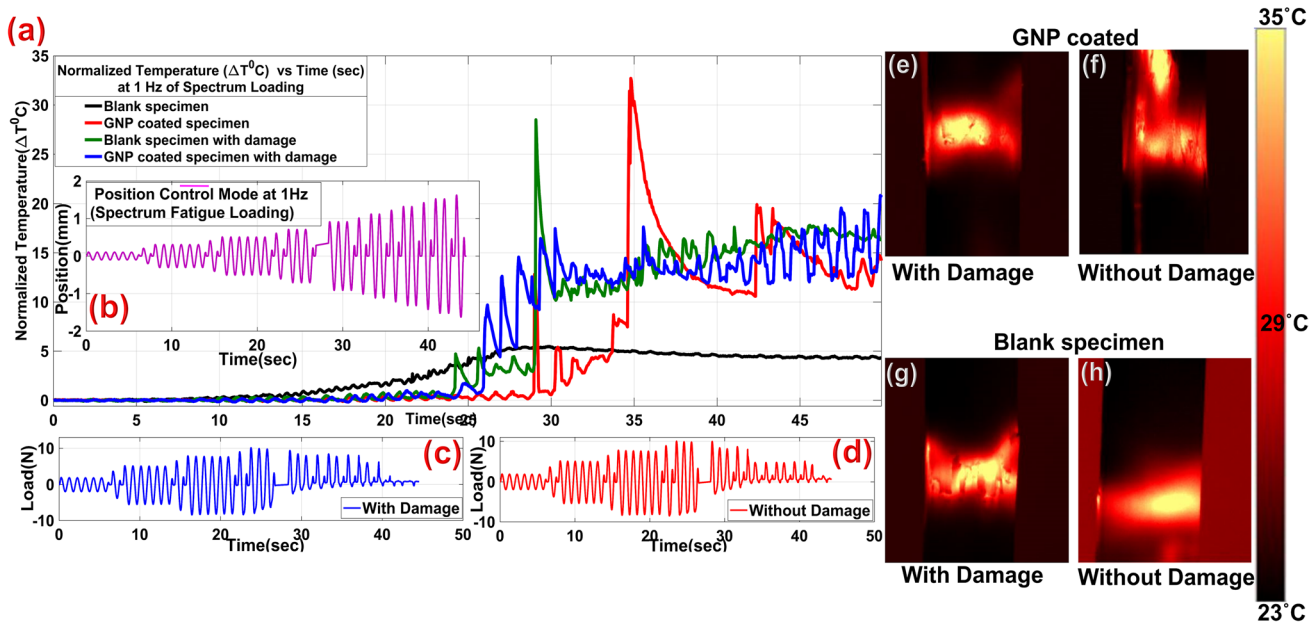

Fig. 10 Normalized Temperature monitoring of GFRP at 1 Hz of spectrum loading: **a** Blank specimen and GNP coated specimen of 110 mm×25 mm (with a damage of 1 mm at the center and without damage) tested for Normalized temp vs Time. **b** Position vs Time during spectrum fatigue at position control mode. **c** and **d** Load vs Time graph till the failure for GNP coated specimen with and without damage for indication of failure. **e** and **f** GNP coated specimen with and without damage till break in spectrum loading. **g** and **h** Blank specimen with and without damage for spectrum loading upto break

Uniaxial Thermography Data

With Damage			Without Damage		
1. 0.1mm/min		Increased (%)	1. 0.1mm/min		Increased (%)
GNP Coated	-0.15°C		GNP Coated	0.2°C	
Blank Specimen	-2.47°C	93.2	Blank Specimen	-1.6°C	112.5
2. 0.5mm/min			2. 0.5mm/min		
GNP Coated	-0.15°C		GNP Coated	-0.13°C	
Blank Specimen	-0.237°C	36.7	Blank Specimen	-0.15°C	13.3
3. 1mm/min			3. 1mm/min		
GNP Coated	-0.16°C		GNP Coated	-0.15°C	
Blank Specimen	-0.68°C	76.4	Blank Specimen	-0.25°C	40

Fatigue Peak Thermography Data

With Damage		Increased (%)	Without Damage		Increased (%)
1. 0.1Hz			1. 0.1Hz		
GNP Coated	9.63°C		GNP Coated	12.43°C	
Blank Specimen	0.45°C	2040	Blank Specimen	-0.08°C	15637.5
2. 1Hz			2. 1Hz		
GNP Coated	9.69°C		GNP Coated	12.81°C	
Blank Specimen	4.71°C	105.73	Blank Specimen	5.27°C	143.07

Fig. 11 Table for quantitative analysis for thermography interpretation in uniaxial loading and 1st break of laminate in terms of temperature in dynamic spectrum loading

°C. Correspondingly, a thermogram can be observed for the specimen with GNP and without GNP coated upon with and without damage specimen in Fig. 10e, f, g and h revealing the surface temperature released during fibers breakage. From the above Fig. 10b, position vs time has been shown, which took 45 s to complete. From Fig. 10c and d, load vs time w.r.t damage has been shown, where failure took place at 39th s and it took 42nd s for specimen without the damage respectively. As seen from the above Fig. 10e and f the failure of the specimen with the damage in mechanical fatigue testing was observed to be at 0.8966 mm and 9.10 N following the 2nd peak of failure at 0.9 mm and 8.215 N. The 3rd peak was observed at 0.9 mm and 7.26 N following the complete failure at 1.05 mm and 3.2 N. Correspondingly, it was observed for temperature peak rise level with an increment of amplitude in spectrum fatigue loading. As seen from above Fig. 10a for the GNP coated specimen with the damage, temperature peak for 1st laminate failure occurred at 17.46 °C following the 2nd peak of failure with the release of temperature at 17.62 °C and maximum temperature is released in 3rd peak at 22.41 °C. Then complete failure took place with the release of temperature 17.38 °C. Similarly, for GNP coated specimen without damage, 1st failure was observed with the release of temperature 12.81 °C following 2nd peak rise in temperature 32.7 °C. The complete failure took place with the release of temperature 19.57 °C. Similarly, blank specimen without a damage was tested for mechanical fatigue loading. The 1st peak for laminate failure took place at 0.903 mm and 10.45 N following 2nd peak of failure at 0.902 mm and 9.56 N. The complete fiber breakage took place at 1.09 mm and 7.7 N following the complete

failure at 1.2 mm and 4.49 N. Correspondingly comparing in terms of temperature, blank specimen without damage for 0.1 Hz, 1st peak of temperature rise was 5.21 °C and then it decreased down to failure 4.44 °C. Similarly, for the specimen with the damage, 1st peak for failure in the laminate was observed with 4.43 °C following 2nd peak at 28.49 °C and then complete failure was observed with reduction of stiffness with temperature 17.41 °C. At 1 Hz, for specimen without GNP without the damage, 1st peak failure was observed at 5.19 °C following the complete failure at 4.24 °C. But for the sample without GNP with the damage, 1st peak was observed at 4.71 °C following 2nd peak of failure at 5.3 °C. Then 3rd peak of failure was observed at 28.49 °C following the complete failure at 4th peak 15.75 °C. Correspondingly, a thermogram can be observed for the specimen with GNP and without GNP coated upon with and without damage specimen in Fig. 9g, h, i and j revealing the surface temperature released during fibers breakage. From Fig. 11, tabulation for quantitative analysis at different spectrum frequency has been shown during first laminate breakage.

5 Conclusion

GFRP composites without damage distributed stresses throughout fibers and matrixes as energy was absorbed during testing but GFRP composites with damage dissipated energy through the damage. This has got a function of displacement rate from 0.1 to 1 mm/min. For GNP skin coated specimen without damage, the temperature rises in 0.1 mm/min, 0.5 mm/min and 1 mm/min are

0.2 °C, − 0.135 °C, − 0.15 °C respectively. Whereas for GNP skin coated specimen with damage, the temperature rises in 0.1 mm/min, 0.5 mm/min and 1 mm/min are 0 °C, − 0.15 °C and − 0.16 °C respectively. Similarly, without damage specimen and without GNP coating, the temperature slowed down to − 1.6 °C, − 0.15 °C and − 0.25 °C. And with damage specimen without GNP coat, temperature slowed down to − 2.47 °C, − 0.237 °C and − 0.68 °C. At 0.1 mm/min, temperature change for blank specimen without damage after GNP coating increased to 112.5% as compared to with damage blank specimen which was 93.2%. Similarly, for 0.5 mm/min, temperature change increased to 13.3% as compared to with damage being at 36.7%. And at 1 mm/min temperature increased to 40% without the damage as compared to 76.4% with the damage. The GNPs of 1 kΩ has caused an increase in the temperature with a displacement rate of 0.1 mm/min and slowly it got reduced with an increase in displacement rate because of Kapitz resistance. But in case of dynamic spectrum loading, there is a lot of friction development between the fibers that leads to temperature rise. For 0.1 Hz spectrum loading, the temperature peak was 12.43 °C and − 0.08 °C in without damage specimen with GNP and without GNP coated specimen, respectively. From 0.1 Hz, with damage specimen, temperature peak was 9.63 °C and 0.45 °C for GNP coated and without coated specimen respectively. Similarly, for 1 Hz specimen temperature peak was 9.69 °C with GNP coated but it reduced down to 4.71 °C in case of without GNP coated. Similarly, for without damage specimen, the temperature was 12.81 °C with GNP coated and it reduced down to 5.27 °C in case of without GNP coated. This later was absorbed by skin coated GNP sensor and captured by IR-camera. GNP smart skin over Blank GFRP composites has shown good thermal signature as compared to blank specimen and can be used to evaluate surface defects and internal damage. Hence, GNP smart skin coating can be used to evaluate surface defects in GFRP composites.

Declarations

Conflict of interest "The authors declare that they have no known competing financial interests or personal relationships that could have appeared to influence the work reported in this paper."

References

1. Nawaz, K., Khan, U., Ul-Haq, N., May, P., O'Neill, A., Coleman, J.N.: Observation of mechanical percolation in functionalized graphene oxide/elastomer composites. Carbon **50**, 4489–4494 (2012). https://doi.org/10.1016/j.carbon.2012.05.029

2. Papageorgiou, D.G., Kinloch, I.A., Young, R.J.: Mechanical properties of graphene and graphene-based nanocomposites. Prog. Mater Sci. **90**, 75–127 (2017). https://doi.org/10.1016/j.pmatsci.2017.07.004

3. Kausar, A.: Emerging trends in poly (methyl methacrylate) containing carbonaceous reinforcements—carbon nanotube, carbon black, and carbon fiber. J. Plast. Film Sheeting **36**, 409–429 (2020). https://doi.org/10.1177/8756087920917177

4. Sethy, D., Makireddi, S., Varghese, F.V., Balasubramaniam, K.: Piezoresistive behaviour of graphene nanoplatelet (GNP)/PMMA spray coated sensors on a polymer matrix composite beam. eXPRESS Polym. Lett. **13**, 1018–1025 (2019). https://doi.org/10.3144/expresspolymlett.2019.88

5. Makireddi, S., Sethy, D., Varghese, F.V., Balasubramaniam, K.: Cyclic loading behaviour and crack monitoring potential of graphene nanoplatelet (GNP) based strain sensors in simple structures. Mater Res. Express **5**, 035701 (2018). https://doi.org/10.1088/2053-1591/aaaf7b

6. Castanedo, C.I., Tarpani, J.R., Maldague, X.P.V.: Nondestructive testing with thermography. Eur. J. Phys. **34**, S91–S109 (2013). https://doi.org/10.1088/0143-0807/34/6/S91

7. He, L., Zhao, Y., Xing, L., Liu, P., Zhang, Y., Wang, Z.: Low infrared emissivity coating based on graphene surface-modified flaky aluminum. Materials **11**, 1502 (2018). https://doi.org/10.3390/ma11091502

8. Wiecek, B.: Review on thermal image processing for passive and active thermography In: *Proceedings of the 2005 IEEE Engineering in Medicine and Biology 27th Annual Conference* Shanghai, China, September 1–4, pp. 686–689 (2005). https://doi.org/10.1109/iembs.2005.1616506

9. Salihoglu, O., Uzlu, H.B., Yakar, O., Aas, S., Balci, O., Kakenov, N., Balci, S., Olcum, S., Süzer, S., Kocabas, C.: Graphene-based adaptive thermal camouflage. Nano Lett. **18**, 4541–4548 (2018). https://doi.org/10.1021/acs.nanolett.8b01746

10. Wen, C.D., Mudawar, I.: Emissivity characteristics of roughened aluminum alloy surfaces and assessment of multispectral radiation thermometry (MRT) emissivity models. Int. J. Heat Mass Transf. **47**, 3591–3605 (2004). https://doi.org/10.1016/j.ijheatmasstransfer.2004.04.025

11. Gong, F., Li, H., Wang, W., Xia, D., Liu, Q., Papavassiliou, D.V., Xu, Z.: Recent advances in graphene-based free-standing films for thermal management: synthesis, properties, and applications. Coatings **8**(63), 1–17 (2018). https://doi.org/10.3390/coatings8020063

12. Balandin, A.A., Ghosh, S., Bao, W., Calizo, I., Teweldebrhan, D., Miao, F., Lau, C.N.: Superior thermal conductivity of single-layer graphene. Nano Lett. **8**(3), 902–907 (2008). https://doi.org/10.1021/nl0731872

13. Zhao, G., Li, X., Huang, M., Zhen, Z., Zhong, Y., Chen, Q., Zhao, X., He, Y., Hu, R., Yang, T., Zhang, R., Li, C., Kong, J., Xu, J.B., Ruoff, R.S., Zhu, H.: The physics and chemistry of graphene-on-surfaces. Chem. Soc. Rev. **46**, 4417–4449 (2017). https://doi.org/10.1039/c7cs00256d

14. Freitag, M., Chiu, H.Y., Steiner, M., Perebeinos, V., Avouris, P.: Thermal infrared emission from biased graphene. Nat. Nanotechnol. **5**, 497–501 (2010). https://doi.org/10.1038/nnano.2010.90

15. Huang, S.Y., Zhao, B., Zhang, K., Yuen, M.M.F., Xu, J.B., Fu, X.Z., Sun, R., Wong, C.P.: Enhanced reduction of graphene oxide on recyclable Cu foils to fabricate graphene films with superior thermal conductivity. Sci. Rep. **5**, 14260 (2015). https://doi.org/10.1038/srep14260

16. Dai, W., Yu, J., Liu, Z., Wang, Y., Song, Y., Lyu, J., Bai, H., Nishimura, K., Jiang, N.: Enhanced thermal conductivity and retained electrical insulation for polyimide composites with SiC

nanowires grown on graphene hybrid fillers. Compos. Part A **76**, 73–81 (2015). https://doi.org/10.1016/j.compositesa.2015.05.017

17. Ganguli, S., Roy, A.K., Anderson, D.P.: Improved thermal conductivity for chemically functionalized exfoliated graphite/epoxy composites. Carbon **465**, 806–817 (2008). https://doi.org/10.1016/j.carbon.2008.02.008

18. Yang, J., Qi, G.Q., Liu, Y., Bao, R.Y., Liu, Z.Y., Yang, W., Xie, B.H., Yang, M.B.: Hybrid graphene aerogels/phase change material composites: thermal conductivity, shape-stabilization and light-to-thermal energy storage. Carbon **100**, 693–702 (2016). https://doi.org/10.1016/j.carbon.2016.01.063

19. Wu, H., Lu, C., Zhang, W., Zhang, X.: Preparation of low-density polyethylene/low-temperature expandable graphite composites with high thermal conductivity by an in-situ expansion melt blending process. Mater. Des. **52**(24), 621–629 (2013). https://doi.org/10.1016/j.matdes.2013.05.056

20. Guo, H., Li, X., Li, B., Wang, J., Wang, S.: Thermal conductivity of graphene/poly (vinylidene fluoride) nanocomposite membrane. Mater. Des. **114**, 355–363 (2017). https://doi.org/10.1016/j.matdes.2016.11.010

21. Kim, S.Y., Ye, J.N., Yu, J.: Thermal conductivity of graphene nanoplatelets filled composites fabricated by solvent-free processing for the excellent filler dispersion and a theoretical approach for the composites containing the geometrized fillers. Compos. Part A **69**, 219–225 (2015). https://doi.org/10.1016/j.compositesa.2014.11.018

22. Hazarika, M., Jana, T.: Graphene nanosheets generated from sulfonated polystyrene/graphene nanocomposite. Compos. Sci. Technol. **87**(5), 94–102 (2013). https://doi.org/10.1016/j.compscitech.2013.08.004

23. Li, X., Linbo, S., Song, N., Shi, L., Ding, P.: Enhanced thermal-conductive and anti-dripping properties of polyamide composites by 3D graphene structures at low filler content. Compos. Part A **88**, 305–314 (2016). https://doi.org/10.1016/j.compositesa.2016.06.007

24. Tsai, M.W., Chuang, T.H., Meng, C.Y., Chang, Y.T., Lee, S.C.: High performance midinfrared narrow-band plasmonic thermal emitter. Appl. Phys. Lett. **89**, 173116 (2006). https://doi.org/10.1063/1.2364860

25. Sethy, D., Makireddi, S., Varghese, F.V., Balasubramaniam, K.: Passive thermo-elastic behaviour of surface enhanced glass-epoxy composites with spray coated graphene nanoplatelets (GNP). Mater. Res. Express **6**, 125044 (2019). https://doi.org/10.1088/2053-1591/ab57ca

26. Liu, L., Zhou, M., Jin, L., Li, L., Mo, Y., Su, G., Li, X., Zhu, H., Tian, Y.: Recent advances in friction and lubrication of graphene and other 2D materials: mechanisms and applications. Friction **7**(3), 199–216 (2019). https://doi.org/10.1007/s40544-019-0268-4

27. Rad, A.V.M., Keller, T., Vassilopoulos, A.P.: Interrupted tension-tension fatigue behavior of angle-ply GFRP composite laminates. Int. J. Fatigue **113**, 377–388 (2018). https://doi.org/10.1016/j.ijfatigue.2018.05.001

28. He, L., Wang, H., Zhu, H., Gu, Y., Li, X., Mao, X.: Thermal properties of PEG/graphene nanoplatelets (GNPs) composite phase change materials with enhanced thermal conductivity and photo-thermal performance. Appl. Sci. **8**, 2613 (2018). https://doi.org/10.3390/app8122613

29. Fu, L., Wang, T., Yu, J., Dai, W., Sun, H., Liu, Z., Sun, R., Jiang, N., Yu, A., Lin, C.T.: An ultrathin high-performance heat spreader fabricated with hydroxylated boron nitride nanosheets. 2D Materials **4**, 025047 (2017). https://doi.org/10.1088/2053-1583/aa636e

30. Hu, N., Wei, L., Wang, Y., Gao, R., Chai, J., Yang, Z., Kong, E.S.-W., Zhang, Y.: Graphene oxide reinforced polyimide nanocomposites via in situ polymerization. J. Nanosci. Nanotechnol. **12**(1), 173–178 (2011). https://doi.org/10.1166/jnn.2011.5144

31. Kim, H., Abdala, A.A., Macosko, C.W.: Graphene/polymer nanocomposites. Macromolecules **43**(16), 6515–6530 (2010). https://doi.org/10.1021/ma100572e

32. Shen, Z.B., Tang, H.L., Li, D.K., Tang, G.J.: Vibration of single-layered graphene sheet-based nanomechanical sensor via nonlocal Kirchhoff plate theory. Comput. Mater. Sci. **61**, 200–205 (2012). https://doi.org/10.1016/j.commatsci.2012.04.003